Research Paper

Site-specifically labeled [89]Zr-DFO-trastuzumab improves immuno-reactivity and tumor uptake for immuno-PET in a subcutaneous HER2-positive xenograft mouse model

Lotte K. Kristensen[1,2]*, Camilla Christensen[2]*, Mette M. Jensen[1,2], Brian J. Agnew[3], Christina Schjöth-Frydendahl[2], Andreas Kjaer[2]✉, Carsten H. Nielsen[1,2]

1. Minerva Imaging, Copenhagen, Denmark
2. Dept. of Clinical Physiology, Nuclear Medicine & PET and Cluster for Molecular Imaging, Dept. of Biomedical Sciences, Rigshospitalet and University of Copenhagen, Denmark
3. Thermo Fisher Scientific, Eugene, OR

*Contributed equally

✉ Corresponding author: Prof. Andreas Kjaer, Dept. of Clinical Physiology, Nuclear Medicine & PET, Rigshospitalet, KF-4012, Blegdamsvej 9, DK-2100 Copenhagen, Denmark. +45 35454216; akjaer@sund.ku.dk; ORCID ID: 0000-0002-2706-5547

Abstract

Antibody-based PET tracers are exceptionally well-suited for determination of the *in vivo* biodistribution and quantification of therapeutic antibodies. The continued expansion in antibody-based therapeutics has accordingly driven the development towards more robust conjugation strategies in order to reliably predict the performance of such agents. We therefore aimed to evaluate the effect of site-specific labeling by enzymatic remodeling on the stability, immuno-reactivity and tumor-targeting properties of the monoclonal antibody (mAb) trastuzumab and compare it to conventional, random labeling in a HER2-positive xenograft mouse model.

Methods: Trastuzumab was conjugated with the *p*-SCN-Bn-Desferrioxamine (SCN-Bn-DFO) chelator randomly on lysine residues or site-specifically on enzymatically modified glycans using either β-galactosidase or endoglycosidase S2 prior to [89]Zr radiolabeling. [89]Zr-DFO-trastuzumab was injected into SK-OV-3 tumor-bearing NMRI nude mice. The antibody dose was titrated with either 100 µg or 500 µg of unlabeled trastuzumab. Mice underwent small animal PET/CT imaging 24, 70 and 120 hours post-injection for longitudinal assessment. Parallel experiments were conducted with an isotype control matched antibody. *In vivo* imaging was supported by conventional *ex vivo* biodistribution and HER2 immuno-histochemistry. Furthermore, site-specifically labeled [89]Zr-DFO-trastuzumab was evaluated in a panel of subcutaneous patient-derived xenograft (PDX) models. Additionally, the affinity, *in vitro* stability and immuno-reactivity were assessed for all tracers.

Results: Site-specific labeling significantly increased PET tumor uptake (One-way ANOVA, *p<0.0001*) at all time-points when compared to random labeling. Mean tumor uptakes were 6.7 ± 1.7, 13.9 ± 3.3 and 15.3 ± 3.8 % injected dose per gram tissue (%ID/g) at 70 hours post-injection, for random, β-galactosidase or endoglycosidase S2 labeled probes, respectively. Co-injection with unlabeled trastuzumab increased the circulation time of tracers but did not alter tumor uptake notably. Site-specific probes presented with a superior *in vitro* stability and immuno-reactivity compared to the randomly labeled probe. *Ex vivo* biodistribution confirmed the data obtained by *in vivo* PET imaging, and site-specific [89]Zr-DFO-trastuzumab successfully detected HER2-positive tumors in PDX mouse models.

Conclusion: [89]Zr-DFO-trastuzumab is well-matched for specific immuno-PET imaging of HER2-positive tumors and site-specific labeling of trastuzumab by the SiteClick™ technology minimizes the impact of the

DFO chelator on immuno-reactivity, stability and biodistribution. These findings support further development of site-specifically radiolabeled mAbs for immuno-PET.

Key words: Positron emission tomography (PET), immuno-PET, site-specific labeling, molecular imaging, HER2

Introduction

Given their extraordinary target-specificity, monoclonal antibodies (mAbs) have emerged as a particularly well-suited platform for development of positron emission tomography (PET) imaging agents. Such antibody-based PET tracers combine the non-invasive quantitative nature of PET with the high selectivity, stability and favorable pharmacokinetic properties of mAbs. PET imaging with radiolabeled mAbs (immuno-PET) serves diagnostic as well as therapeutic purposes [1,2], with the ability to image and track the biodistribution of therapeutic antibodies and radioimmunoconjugates. Furthermore, immuno-PET imaging agents are ideal for *in vivo* evaluation of biomarker expression providing phenotypic information related to primary and metastatic lesions, thus ultimately guiding therapy decisions.

The relatively slow pharmacokinetics of intact antibodies necessitates a radioisotope with a suitable physical half-life, such as Zirconium-89 (^{89}Zr, $T_{1/2}$=78.4 hours). Zirconium-89 decays to yttrium-89 via beta decay with 22.7 % positron emission. In addition to 511 keV annihilation radiation, the decay gives rise to a 99% abundant 909 keV gamma. The desferrioxamine (DFO) chelator [3] has long been the preferred choice for stable coupling of ^{89}Zr to preclinical and clinical immuno-PET imaging agents [4–8]. The need for stable chelation chemistry in the development of ^{89}Zr-immuno-PET imaging probes is highlighted by the fact that uncomplexed ^{89}Zr localizes to bone in mice and thereby possibly delivers a high non-targeted radiation dose, which has led to a continued research into the development of improved chelating agents [9–11]. In addition, the majority of known chelator conjugation strategies rely on reactions with amino acids which can lead to an uneven and random distribution of chelates. Even conventional methodology for chelator conjugation to mAbs can suffer from several shortcomings such as potential loss of immuno-reactivity, inadequately defined conjugates as well as lack of reproducibility [12]. Together with the steady expansion and use of antibody-based therapies for cancer, such as antibody-drug-conjugates (ADCs) and radio-immunotherapy agents, this has increased attention towards alternative conjugation strategies such as site-specific conjugation [2,13,14].

Site-specific conjugation allows for a single, uniform product as opposed to a heterogeneous mixture of conjugates resulting from the conventional random conjugation methodology [15]. By harnessing an explicit site, distant from the antigen-binding region, the site-specific strategy offers stoichiometric control as well as minimal loss of immuno-reactivity. The impact of site-specific conjugation on *in vivo* behavior has been confirmed in multiple applications such as antibody-drug conjugation [16,17] and molecular imaging [12,18–21].

Several technologies for site-specificity have emerged over the past years by utilizing approaches such as cysteine engineering [19,22], click chemistry [23,24] and glycan remodeling [25,26]. Cysteine engineering of antibodies is an elegant way of tailoring both the location and number of conjugates but is equally a complex and constrained system adding expense to the conjugation process. Remodeling of the heavy chain glycans of antibodies is an interesting platform offering highly specific conjugation distal to the antigen-binding region in a robust and reproducible manner [25–27]. By exploiting two conserved glycosylation sites on heavy chain glycans this site-specific modification (SiteClick™) approach [25] is a robust technique that can be applied on various IgG's across species while requiring only minimal optimization. In brief, the SiteClick™ radiolabeling procedure uses enzymatic processes to incorporate an activated azide into the heavy chain glycans enabling click-conjugation of a payload such as the DFO chelator.

We hereby demonstrate the use of the SiteClick™ technology to the production of site-specifically labeled immuno-PET imaging probes and compare them to a conventional, randomly labeled probe. Given that trastuzumab (Herceptin®) is one of the most widely used mAbs in clinical oncology and our experience in trastuzumab radiolabeling [28], we chose HER2/trastuzumab as the model system to investigate the effect of site-specific labeling. We paired trastuzumab with ^{89}Zr to reach optimal target-to-background ratios and applied it to the HER2-positive SK-OV-3 ovarian adenocarcinoma mouse model. This site-specific conjugation methodology produced well-defined constructs with improved immuno-reactivity,

stability and tumor uptake when compared to their randomly labeled counterparts.

Materials and Methods

Cell culture and animal models

SK-OV-3 ovarian adenocarcinoma cells (ATCC HTB-77, LGC standards) were cultured in McCoy's 5a Modified Medium supplemented with 10% FBS and 1% penicillin-streptomycin at 37 °C and 5% CO_2. Cells were harvested in their exponential growth phase and resuspended 1:1 in complete growth media and Matrigel™ (BD Biosciences) at a concentration of 5×10^7 cells/mL. 100 uL of the cell suspension (5×10^6 cells/tumor) was injected subcutaneously into the flanks (2 tumors/mouse) above the hind limbs in 7-week old female NMRI nude mice (Taconic, Denmark). Tumors were grown until ~ 200 mm^3 prior to imaging experiments and mice were randomized into 11 groups (N=4/group).

The ST562 (gastric), ST2789B (breast), ST518 (breast), ST928B (breast) and ST1616B (breast) PDX models (START, San Antonio, TX, USA) were established by subcutaneous passage of tumor pieces (1 tumor/mouse) into the flanks in 7-week old female NMRI nude mice. All animal procedures were conducted with approval by the National Animal Experiments Inspectorate (license no. 2016-15-0201-00920).

Antibody conjugation and radiolabeling

Trastuzumab (Herceptin®, Roche, Basel, Switzerland) was either site-specifically modified by enzymatic reactions or randomly conjugated to *p*-SCN-Bn-Desferrioxamine (SCN-Bn-DFO, Macrocyclics). β-(1-4) galactosidase, GalT enzyme and UDP-GalNAz substrate were obtained from Thermo Fisher Scientific (OR, USA) and endoglycosidase S2 was purchased from Genovis (Lund, Sweden).

One mg of purified trastuzumab was incubated for either 6 hours at 37 ºC with β-(1-4) galactosidase (8 μL, 2U/mL) or 2 hours at 37 ºC with endoglycosidase S2 (5 μL) in a reaction volume of 100 μL. After incubation, GalT enzyme (20 μL, 2 mg/mL), UDP-GalNAz substrate (20 μL, 40 mM) and MnCl₂ in 0.1 M HCl (2 μL, 1 M) were added to a final reaction volume of 200 μL, and the mixture was incubated overnight at 30 ºC. Excess UDP-GalNAz and GalT enzyme were removed and the buffer was exchanged into Tris-buffered Saline (TBS) using Amicon ULTRA 50 kD MW cut-off spin filters. Site-specifically modified trastuzumab was conjugated to DIBO-DFO (40 μL, 4 mM) in 35 molar excess overnight at 25 ºC and ultimately purified using Amicon ULTRA 50 kD MW cut-off spin filters. Accordingly, randomly labeled trastuzumab was prepared by incubating 5 mg of purified trastuzumab (27.5 nmol, 170 μL) with 5 molar excess DFO-Bz-NCS dissolved in DMSO in 0.1 M NaHCO₃ (1 hour, 37 ºC, pH=9.0) followed by PD-10 purification (GE Healthcare, IL, USA) into PBS. Additionally, a final version of DFO-trastuzumab was prepared by treating 1 mg trastuzumab with endoglycosidase S2 followed by random conjugation according to the methods described above. Thus, four different conjugates of DFO-trastuzumab were obtained. Concurrently, an isotype control matched antibody (Human IgG1, #BE0297, BioXcell, USA) was either site-specifically conjugated by the endoS2 method or randomly conjugated to DFO by the protocols described above. Aliquots of 200 μg of DFO-trastuzumab and DFO-IgG1 were stored until radiolabeling at -80 ºC. Degree of labeling (DOL) was determined for the following conjugates by mass spectrometry: random, β-Gal and endoS2 modified DFO-trastuzumab.

^{89}Zr-oxalate (PerkinElmer, the Netherlands) was neutralized to pH ~7 with 1 M Na₂CO₃ prior to labeling. 200 μg of modified and conjugated trastuzumab or IgG1 was incubated with 150 MBq neutralized ^{89}Zr-oxalate (1 hour, 37 ºC, pH=7.0) followed by PD10 purification into PBS. The radiochemical yield and purity at end-of-synthesis (EOS) were determined by radio-thin-layer chromatography (radio-TLC) using an eluent of 50 mM EDTA (pH 5.5) on silica gel 60 TLC plates, where the antibody construct remains at the baseline, while ^{89}Zr^{4+} ions and [^{89}Zr]-EDTA elute with the solvent front. Purity was also assessed by size-exclusion-chromatography – high-performance-liquid-chromatography (SEC-HPLC) by using an isocratic method with 0.1 M phosphate buffer, pH=7 as mobile phase and a flowrate of 1 mL/min.

Flow cytometry, immuno-reactivity and stability measures

The binding affinity of the different DFO-trastuzumab conjugates was evaluated using flow cytometry. In brief, 0.3×10^6 SK-OV-3 cells were incubated with increasing concentrations (0.39-100 nM) of unlabeled trastuzumab, DFO-trastuzumab (random), DFO-trastuzumab (β-Gal) and DFO-trastuzumab (endoS2) for 1 hour at 4 ºC. Cells were washed twice in FACS buffer (1% BSA, 0.5 mM EDTA in PBS) and stained for 30 min at 4 ºC with AF488-anti-human IgG (#A11013, Life Technologies). Cell-associated fluorescent intensity was quantified using FACSCanto II (BD Biosciences, New Jersey, USA) and data analyzed using FlowJo Software (v10.0.7, Tree Star, OR, USA).

The immuno-reactivity of the different versions of ^{89}Zr-DFO-trastuzumab was assessed according to

the Lindmo assay [29]. Increasing concentrations of SK-OV-3 cells (1.25×10^6 – 4.5×10^7 cells/mL) were incubated with 6 nM ^{89}Zr-DFO-trastuzumab for 3 hours at 4 ºC. Cells were centrifuged at 500g for 5 minutes and the supernatants and pellets counted in a gamma counter (Wizard^2, PerkinElmer, MA, USA). Cell-associated radioactivity was calculated as the ratio of cell-bound radioactivity to the total amount of radioactivity added.

The *in vitro* stability of labeled probes was evaluated up to 7 days after radiolabeling in either PBS (4 ºC) or mouse plasma (37 ºC). A total of 2 MBq of ^{89}Zr-DFO-trastuzumab was incubated with 0.5 mL PBS or plasma and a sample withdrawn at least every other day. The radiochemical stability in buffer and plasma was determined by radio-TLC as described above.

Small animal PET/CT imaging

Longitudinal small animal PET/CT imaging was conducted on an Inveon Multimodality PET/CT scanner (Siemens, Germany). Mice bearing SK-OV-3 tumors (N=4/tracer) were injected intravenously immediately after EOS via the tail vein with 2.08 ± 0.2 [range: 1.2 - 2.3] MBq ^{89}Zr-DFO-trastuzumab (random, β-Gal and endoS2 variants) diluted in 0.9% sterile NaCl prior to injection (200 μL total volume). Concurrently, the protein dose was 8.9 ± 0.3 [range: 6.4 - 13.2] μg. A group of mice received a co-injection of 100 μg (N=4/tracer) or 500 μg (N=4/tracer) unlabeled trastuzumab for random, β-Gal and endoS2 ^{89}Zr-DFO-trastuzumab variants. For isotype control imaging, mice bearing SK-OV-3 tumors (N=4/tracer) were injected intravenously with 2.04 ± 0.02 [range: 1.95 - 2.1] MBq ^{89}Zr-DFO-IgG1 (random and endoS2 variants) diluted in 0.9% sterile NaCl prior to injection (200 μL total volume). Concurrently, the protein dose was 8.9 ± 0.25 [range: 8.5 - 9.3] μg. Mice bearing PDX tumors were injected with 1.15 ± 0.18 MBq ^{89}Zr-DFO-trastuzumab (endoS2) diluted in 0.9% sterile NaCl prior to injection (200 μL total volume). Concurrently, the protein dose was 7.7 ± 0.26 [range: 6.4 - 13.2] μg.

Mice were anesthetized with sevoflurane (4% in 65% N_2, 35% O_2) during PET/CT imaging. Static PET data was acquired in list mode at 24, 70 and 120 hours (acquisition time 300, 600 and 900 s respectively) post-injection (^{89}Zr-DFO-trastuzumab and ^{89}Zr-DFO-IgG1). PET imaging in PDX models was conducted 70 hours post-injection (acquisition time 600 s). Images were reconstructed using a 3D maximum a posteriori algorithm (MAP) with CT based attenuation correction. Image analysis (Inveon Software, Siemens) was performed by drawing CT based region of interests (ROIs). The uptake of

^{89}Zr-DFO-trastuzumab was quantified as % injected dose per gram tissue (%ID/g).

Ex vivo biodistribution

Mice were euthanized after the last imaging session and underwent conventional *ex vivo* biodistribution. Tumors and organs were resected, weighed and the radioactivity counted in a gamma counter (Wizard^2, PerkinElmer). Tumors were fixed in 4% paraformaldehyde for 24 hours and subsequently transferred to 70% ethanol for immunohistochemical analysis.

Immunohistochemistry

Formalin-fixed paraffin-embedded tumors were sectioned at 4 μm, deparaffinized, rehydrated and microwaved in citrate buffer pH=6 for epitope retrieval. Sections were blocked in 2% bovine serum albumin (BSA) in PBS and incubated with anti-ERBB2 (#HPA001383, Sigma Aldrich) at 1:400 dilution for 1 hour at room temperature. Primary antibody was detected using the EnVision+ System-HRP Labeled Polymer and Liquid DAB+ Substrate Chromogen System (Agilent Technologies, California, USA) and sections were counterstained with Mayer's Hematoxylin (Region H Apotek, Denmark). Tumors from each group were stained in the same analysis and HER2 expression was graded according to the HercepTest™ Interpretation Manual (Agilent Technologies, CA, USA) [30].

Statistical analyses

Data are expressed as mean ± SEM. The effect of conjugation method on tumor PET uptake was evaluated by 2-way ANOVA corrected for multiple comparisons (Tukey). One-way ANOVA with *post hoc* test corrected for multiple comparisons (Tukey) was applied to test for differences in tumor volumes and body weight between groups (randomization) and the effect of conjugation method on biodistribution. *P* values ≤ 0.05 were considered statistically significant. Statistical analyses were performed using GraphPad Prism 7.0c (California, USA).

Results

Antibody conjugation and radiolabeling

Trastuzumab was successfully purified and conjugated to DFO by 4 alternate methods: randomly on lysine residues (random), site-specifically using ß-(1-4) galactosidase (β-Gal), site-specifically using endoglycosidase S2 (endoS2) or randomly after site-specific endoS2 cleavage (endoS2-R), (Figure 1A). The immuno-conjugates were labeled with ^{89}Zr with a radiochemical yield of 37.4 ± 3.8, 32.6 ± 4.3, 23.9 ± 2.2 and 22.7 ± 7.3 MBq, respectively. Human IgG1 was

labeled with a radiochemical yield of 32.0 (random) and 15.9 (endoS2) MBq. Radiochemical purity was assessed by radio-TLC and was >99% for all versions of ^{89}Zr-DFO-trastuzumab and ^{89}Zr-DFO-IgG1. Figure 1B shows a representative SEC-HPLC chromatogram of endoS2 modified ^{89}Zr-DFO-trastuzumab. Less than 5% aggregation at EOS for all tracers were observed (data not shown). The specific activity of ^{89}Zr-DFO-trastuzumab was 279.1 ± 28.1 (random), 243.3 ± 31.9 (β-Gal), 178.1 ± 16.4 (endoS2) and 169.4 ± 54.5 (endoS2-R) MBq/mg. The specific activity of ^{89}Zr-DFO-IgG1 was 238.8 (random) and 227.1 (endoS2) MBq/mg. DOL was 0-6 (random), 4 (β-Gal) and 2 (endoS2) as determined by mass spectrometry and was not determined for endoS2-R. See Table 1 for specifications of each tracer.

In vitro evaluation of DFO-trastuzumab

Following chelator conjugation, an *in vitro* binding assay was performed to investigate the effect of chelation methodology on affinity of trastuzumab towards HER2 (Figure 1C). Unlabeled trastuzumab,

random, β-Gal and endoS2 modified DFO-trastuzumab all showed affinities in the nanomolar range. Unlabeled trastuzumab presented with a K_D of 1.09 nM, randomly labeled trastuzumab 1.55 nM and site-specific trastuzumab tracers (β-Gal and endoS2) both exhibited a K_D of 1.45 nM.

Table 1: Specification of tracers

	^{89}Zr-DFO-trastuzumab				^{89}Zr-DFO-IgG1	
	Random	ß-Gal	EndoS2	EndoS2-R	Random	EndoS2
Radiochemical yield (MBq)	37.4 ± 3.8	32.6 ± 4.28	23.9 ± 2.19	22.7 ± 7.3	32.0	15.9
Purity TLC (%)	>99	>99	>99	>99	>99	>99
Aggregates at EOS (%)	≤ 5	≤ 5	≤ 5	≤ 5	≤ 5	≤ 5
Specific activity (MBq/mg)	279.1 ± 28.11	243.3 ± 31.92	178.11 ± 16.38	169.40 ± 54.48	238.8	227.1
Immunoreactivity (%)	80	93	93	82	-	-
Activity injected (MBq)	2.3 ± 0.04	2.2 ± 0.02	1.6 ± 0.06	2.2 ± 0.1	2.1 ± 0.08	2.0 ± 0.05
Protein dose injected (µg)	8.5 ± 0.21	8.3 ± 0.18	8.9 ± 0.06	9.6 ± 0.44	8.9 ± 0.36	8.9 ± 0.21
Degree of labeling	0-6	4	2	-	-	-

Values are mean ± SEM
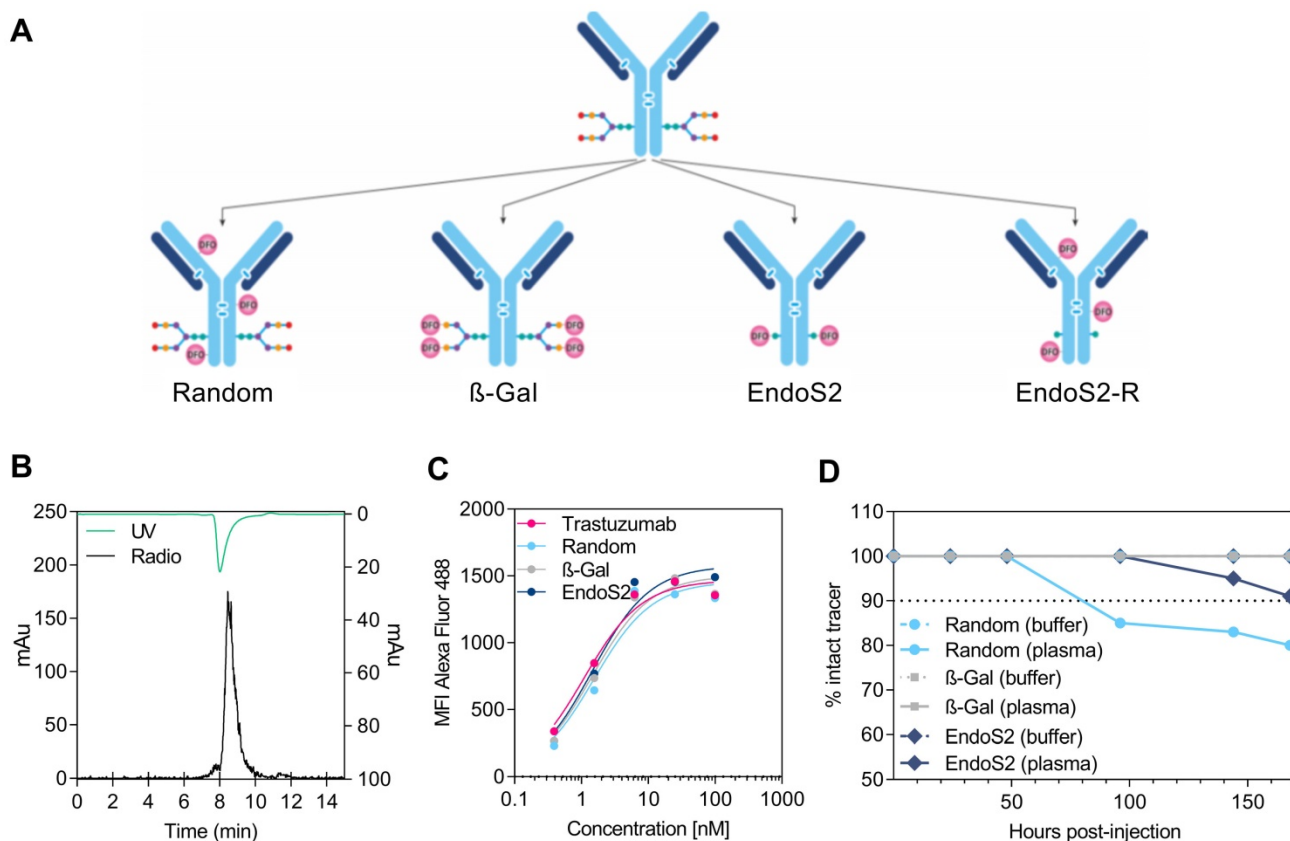
Figure 1: Radiochemistry and in vitro evaluation of ^{89}Zr-DFO-trastuzumab. (A) Schematic illustration of the 4 alternate ways of DFO conjugation to trastuzumab: (1) randomly on lysine residues (random), site-specifically on enzymatically treated glycans using either (2) β-galactosidase (β-Gal) or (3) endoglycosidase S2 (endoS2), or randomly on lysine residues after endoS2 modification (endoS2-R). (B) Representative HPLC chromatogram of endoS2 modified ^{89}Zr-DFO-trastuzumab after PD10 purification. (C) Median fluorescent intensity (MFI) of SK-OV-3 cells incubated with increasing concentrations of unlabeled, random, β-Gal and endoS2 modified trastuzumab. (D) Radio-TLC analysis of tracer stability in plasma and buffer up to 168 hours post-labeling.

The *in vitro* binding characteristics of radiolabeled trastuzumab was also assessed by the cell-binding assay described by Lindmo *et al.* The immuno-reactive fraction was for both site-specifically labeled trastuzumab 93%, whereas the immuno-reactivity was 80% and 82% for randomly and endoS2-R labeled trastuzumab, respectively. The Lindmo binding data of all ^{89}Zr-DFO-trastuzumab tracers are depicted in Figure S1.

^{89}Zr-DFO complex of ^{89}Zr-DFO-trastuzumab was stable in buffer for all tracers with >99% intact tracer after 168 hours of incubation (Figure 1D). This was also the case for β-Gal modified ^{89}Zr-DFO-trastuzumab in plasma, whereas ^{89}Zr-DFO-trastuzumab (endoS2) decreased to 91% and ^{89}Zr-DFO-trastuzumab (random) decreased to 80% after 168 hours in plasma.

Increased uptake of site-specifically labeled trastuzumab in SK-OV-3 tumors

The *in vivo* tumor targeting and distribution of the different ^{89}Zr-DFO-trastuzumab conjugates were assessed by longitudinal PET/CT imaging in SK-OV-3 tumor-bearing mice randomized into 11 groups (N=4/group). No difference in tumor volume was found between the groups at randomization (*p=0.73*), Figure S2. Mice were subjected to PET/CT imaging 24, 70 and 120 hours after injection of ^{89}Zr-DFO-trastuzumab. Representative images of mice from each group 70 hours post-injection clearly illustrate targeting of ^{89}Zr-DFO-trastuzumab to the HER2 expressing SK-OV-3 tumors (Figure 2A). ROI analysis of PET images was used to quantify the temporal uptake in tumors (Figure 2C&D) as well as in the heart, liver, kidney and muscle (Figure 2B).
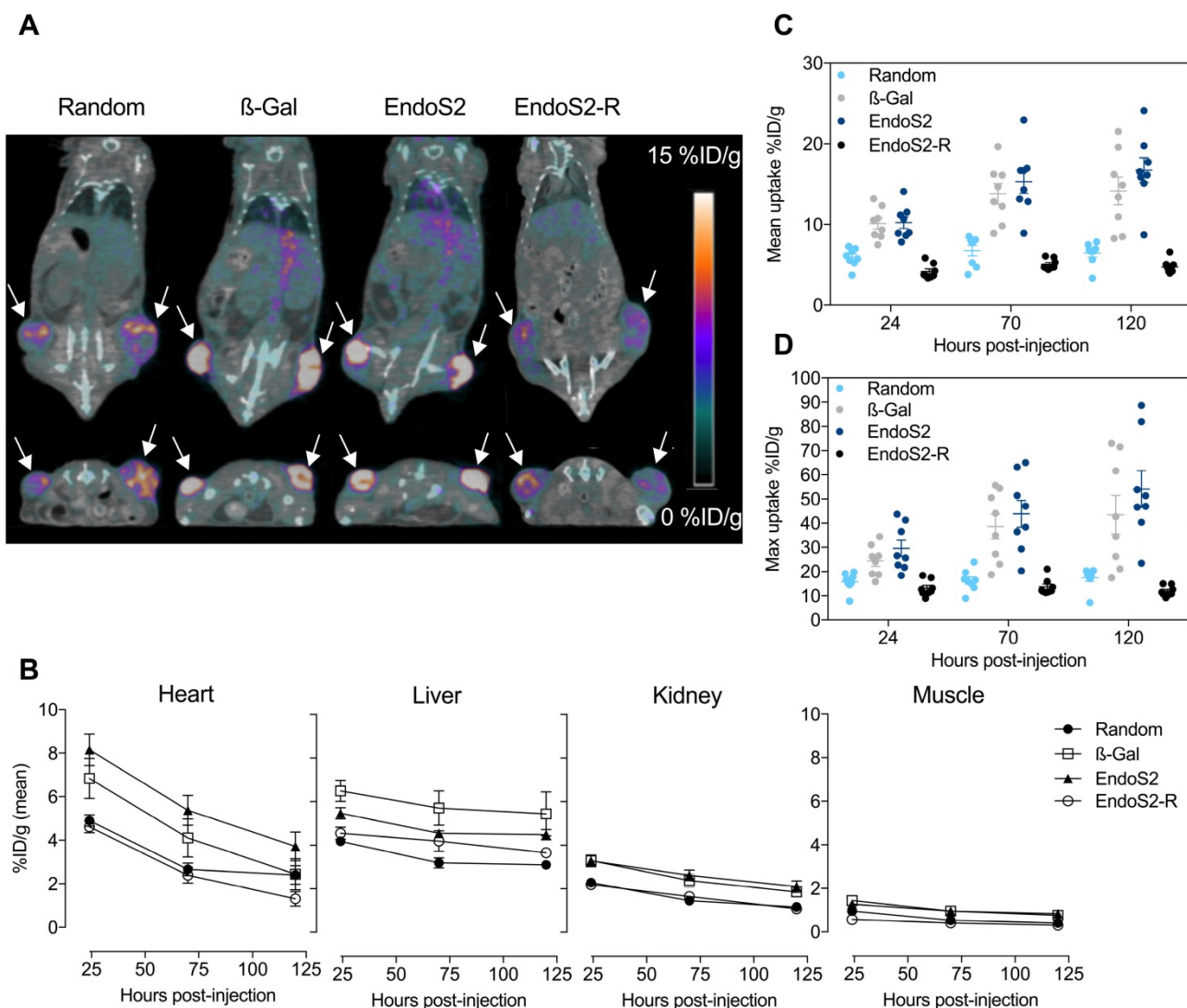
Figure 2: Longitudinal PET/CT imaging in SK-OV-3 xenograft bearing mice. (A) Representative coronal (top) and axial (bottom) images 70 hours post-injection of random, β-Gal, endoS2 and endoS2-R modified ^{89}Zr-DFO-trastuzumab. Arrows designate the tumors. (B) Image-derived biodistribution of ^{89}Zr-DFO-trastuzumab in major organs over the imaging time-course (N=4/tracer). (C) Mean and (D) maximum tumor uptakes at 24, 70 and 120 hours post-injection of tracers (N=4/tracer).

Mean (Figure 2C) and maximum (Figure 2D) tumor uptake values were highly dependent on which conjugation method was applied. For ^{89}Zr-DFO-trastuzumab (random) the accumulation in tumors increased from 5.9 ± 0.4 to 6.5 ± 0.5 %ID/g from the initial to the final time-points. Tumor uptake of site-specific probes increased from 10.1 ± 0.7 to 14.2 ± 1.7 %ID/g and 10.2 ± 0.7 to 16.7 ± 1.5 %ID/g for β-Gal and endoS2 labeled ^{89}Zr-DFO-trastuzumab, respectively. Image-contrast did not increase beyond the 70-hour time-point for any of the tracers. Maximum tumor uptake values showed a similar profile, increasing from 15.8 ± 1.3 to 17.5 ± 1.5 %ID/g (random), 24.5 ± 2.7 to 43.5 ± 7.9 %ID/g (β-Gal) and 29.6 ± 3.4 to 54.2 ± 7.6 %ID/g (endoS2). Compared with random labeling, site-specific labeling showed a higher tumor uptake when measured by PET ($p<0.0001$) at all time-points. *Ex vivo* IHC analysis in SK-OV-3 tumors revealed no difference in HER2 expression between groups receiving random, β-Gal and endoS2 modified ^{89}Zr-DFO-trastuzumab (Figure S3).

Image-derived biodistribution throughout the imaging time-course (Figure 2B) indicated a slower clearance profile for site-specifically labeled trastuzumab when compared to randomly labeled trastuzumab. Both site-specific tracers (β-Gal and endoS2) presented with a similar pharmacokinetic profile with high retention in blood and highly perfused organs such as the liver and kidneys. Uptake in muscle was similar for all tracers.

Ex vivo biodistribution and effect of dose-escalation

Conventional *ex vivo* biodistribution was performed after the last imaging session. The *ex vivo* biodistribution confirmed the *in vivo* imaging results, with key differences in blood pool and tumor uptake among different versions of ^{89}Zr-DFO-trastuzumab (Figure 3). Tumor-to-blood and tumor-to-muscle ratios 120 hours post-injection are listed in Table S1. Tumor uptake of site-specific probes was significantly higher ($p<0.01$) compared with randomly labeled ^{89}Zr-DFO-trastuzumab, presenting with 10.9 ± 1.3 %ID/g (random), 24.1 ± 4.3 %ID/g (β-Gal) and 30.7 ± 3.1 %ID/g (endoS2) at the 120-hour time-point. Further, tumor-to-muscle ratios were increased for site-specific variants (31.5 ± 4.8 and 49.9 ± 6.3 for β-Gal and endoS2, respectively) when compared to randomly labeled ^{89}Zr-DFO-trastuzumab (23.3 ± 2.7). In addition, site-specific ^{89}Zr-DFO-trastuzumab showed an elevated blood pool of 3.9 ± 1.4 %ID/g (β-Gal) and 5.8 ± 0.6 %ID/g (endoS2, $p=0.011$) compared to randomly labeled trastuzumab (2.13 ± 0.3 %ID/g). The *in vivo* stability of probes was also

confirmed by the fairly low amount of ^{89}Zr residing in bone (~2%) for all the tracers, which contrasts greatly to the group receiving free ^{89}Zr (14 %ID/g). Non-tumor non-specific uptake did not significantly differ between the probes except in terms of liver uptake ($p=0.049$, random vs. β-Gal).
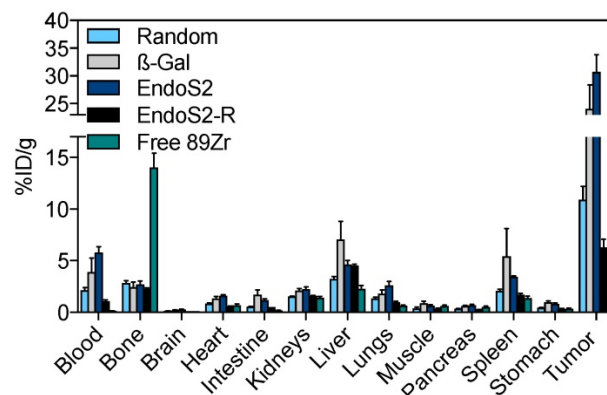
Figure 3: Ex vivo biodistribution. Ex vivo biodistribution 120 hours after injection of random, β-Gal, endoS2 and endoS2-R modified ^{89}Zr-DFO-trastuzumab or free ^{89}Zr in SK-OV-3 tumor-bearing mice (N=4/tracer).

Co-injection with unlabeled trastuzumab did not alter the distribution of ^{89}Zr-DFO-trastuzumab considerably for any of the probes at the 120-hour time-point (Table 2). Notably, the tumor uptake of ^{89}Zr-labeled trastuzumab variants was not affected by antibody dose in the tested range apart from the tumor-to-muscle ratio of endoS2 that decreased from 49.9 ± 6.3 to 27.7 ± 4.1 with 500 µg co-dose (Table S1).

Table 2: Protein dose-escalation ex vivo biodistribution of ^{89}Zr-DFO-trastuzumab

	Organs (%ID/g)								
	Blood	Bone	Heart	Kidneys	Liver	Lungs	Muscle	Spleen	Tumor
Random	2.13 ± 0.3	2.82 ± 0.2	0.84 ± 0.1	1.55 ± 0.1	3.24 ± 0.2	1.34 ± 0.1	0.4 ± 0.1	2.08 ± 0.2	10.9 ± 1.3
Random+100 µg	1.66 ± 0.3	2.71 ± 0.2	0.97 ± 0.1	1.81 ± 0.2	3.22 ± 0.2	1.21 ± 0.1	0.54 ± 0.1	4.56 ± 0.6	10.4 ± 0.8
Random+500 µg	3.13 ± 0.5	2.58 ± 0.2	1.17 ± 0.1	1.88 ± 0.1	2.54 ± 0.2	1.97 ± 0.2	0.43 ± 0.1	2.83 ± 0.6	9.9 ± 1.0
β-Gal	3.90 ± 1.4	2.45 ± 0.5	1.34 ± 0.2	2.12 ± 0.2	7.11 ± 1.8	1.81 ± 0.3	0.89 ± 0.2	5.44 ± 2.7	24.1 ± 4.3
β-Gal+100 µg	3.8 ± 1.1	2.26 ± 0.1	1.49 ± 0.2	2.02 ± 0.2	4.5 ± 0.2	2.16 ± 0.2	0.78 ± 0.1	4.3 ± 0.8	25.2 ± 1.6
β-Gal+500 µg	6.58 ± 1.1	1.92 ± 0.6	2.14 ± 0.2	2.34 ± 0.2	3.42 ± 0.2	2.86 ± 0.4	0.81 ± 0.2	4.66 ± 0.6	24.4 ± 1.9
EndoS2	5.8 ± 0.6	2.71 ± 0.3	1.63 ± 0.1	2.23 ± 0.2	4.64 ± 0.4	2.6 ± 0.4	0.66 ± 0.1	3.43 ± 0.1	30.7 ± 3.1
EndoS2+100 µg	5.42 ± 1.1	2.32 ± 0.4	1.93 ± 0.1	2.57 ± 0.2	2.77 ± 0.2	2.8 ± 0.4	1.0 ± 0.3	2.93 ± 0.5	28.3 ± 2.9
EndoS2+500 µg	6.1 ± 0.2	2.7 ± 0.1	2.14 ± 0.1	2.86 ± 0.2	3.1 ± 0.5	3.42 ± 0.2	1.0 ± 0.2	8.14 ± 2.0	24.4 ± 1.9

Values are mean ± SEM

HER2 expression across PDX models detected by site-specific ^{89}Zr-DFO-trastuzumab

The ability of randomly labeled ^{89}Zr-DFO-trastuzumab to reliably detect and quantify HER2 expression has previously been well

characterized both preclinically [5,31] as well as clinically [7,32]. To verify that site-specific [89]Zr-DFO-trastuzumab possesses similar targeting properties, endoS2 modified [89]Zr-DFO-trastuzumab PET/CT imaging was applied to a panel of PDX models with varying HER2 expression (Figure 4). Site-specific [89]Zr-DFO-trastuzumab was evaluated at the optimal imaging time-point (70 hours post-injection) and successfully detected HER2 expression in the ST1616B (breast), ST2789B (breast), ST928B (breast), ST562 (gastric) and ST518 (breast) model (N=2-3/model). Representative PET/CT images and immunohistochemical sections stained for HER2 from the same mouse are presented in Figure 4A. Quantitative ROI analysis revealed an average tumor uptake of 5.3 ± 0.6, 5.8 ± 0.8, 11.8 ± 3.1, 13.3 ± 1.1 and 15.0 ± 1.8 %ID/g for the ST518, ST562, ST928B, ST2789B and ST1616B model respectively (Figure 4B). High HER2 expression was observed for the ST1616B model (HER2 3+), moderate expression for the ST2789B and ST562 (HER2 2+) models and lowest expression was observed for the ST928B (HER2 1+) and ST518 (HER2 0+) PDX models. Although not correlating directly, the highest *in vivo* tumor uptake of [89]Zr-DFO-trastuzumab (endoS2) was overall detected in ST1616B and ST2789B, intermediate uptake in ST928B and ST562 models and the lowest uptake in the ST518 model.

EndoS2 cleavage does not alter stability and uptake of randomly labeled trastuzumab

We assessed whether enzymatic cleavage prior to random labeling of trastuzumab affected the distribution and tumor uptake of [89]Zr-DFO-trastuzumab (endoS2-R) since glycosylation in the Fc region is known to influence the stability of monoclonal antibodies. Mean tumor uptake of endoS2-R modified [89]Zr-DFO-trastuzumab was 4.2 ± 0.3, 5.1 ± 0.2 and 4.7 ± 0.3 %ID/g for the 24, 70 and 120-hour time-point, respectively. Maximum tumor uptake was 13.1 ± 1.1, 13.7 ± 1.2 and 11.9 ± 0.7 %ID/g for the 24, 70 and 120-hour time-point respectively. EndoS2 modification of trastuzumab prior to random DFO conjugation did not alter either tumor uptake (Figure 2C&D) or distribution of the tracer (Figure 2B). Instead, a similar uptake pattern when compared to the randomly labeled trastuzumab was observed (*p=0.1095*). Concordantly, [89]Zr-DFO-trastuzumab (endoS2-R) presented with an immuno-reactive fraction of 82% (Figure S1D).

Site-specific labeling and PET/CT imaging of isotype control matched antibody

The non-specific uptake of randomly versus site-specifically labeled probes (endoS2) was evaluated by PET/CT imaging with an isotype control matched antibody (human IgG1) in SK-OV-3 tumor-bearing mice. Mice were subjected to PET/CT imaging 24, 70 and 120 hours after injection of [89]Zr-DFO-IgG1. ROI analysis of PET images was used to quantify the temporal uptake in tumors (Figure S4A&B) as well as heart, liver, kidney and muscle (Figure S4C).
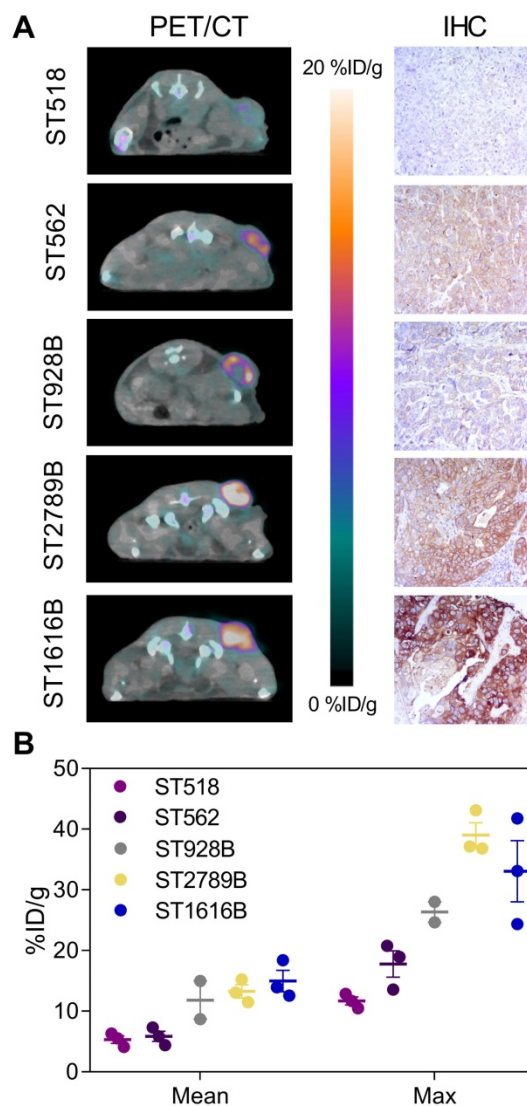
Figure 4: Site-specific [89]Zr-DFO-trastuzumab PET/CT imaging in PDX models with varying HER2 expression. (A) Representative axial PET/CT images of [89]Zr-DFO-trastuzumab (endoS2) tumor uptake in ST518 (breast), ST562 (gastric), ST928B (breast), ST2789B (breast) and ST1616B (breast) PDX models 70 hours post-injection (left). Corresponding ex vivo HER2 immunohistochemical (IHC) analysis of same mouse (right). (B) Quantitative mean and maximum uptake of endoS2 modified [89]Zr-DFO-trastuzumab in tumors of the various PDX models 70 hours post-injection (N=2-3/model).

A decrease in the tumor uptake was observed for both probes over the imaging time-course. Mean tumor uptake of [89]Zr-DFO-IgG1 (random) decreased from 3.3 ± 0.4 to 0.78 ± 0.09 %ID/g from the 24 to the 120-hour time-point. Similarly, mean tumor uptake of [89]Zr-DFO-IgG1 (endoS2) decreased from 3.3 ± 0.2 to

0.9 ± 0.05 %ID/g. Maximum tumor uptake of [89]Zr-DFO-IgG1 decreased from 9.3 ± 2.0 to 1.8 ± 0.2 (random) and from 7.6 ± 0.6 to 2.0 ± 0.2 %ID/g (endoS2) from 24 to 120 hours post-injection. No difference in mean (*p=0.8241*) and maximum (*p=0.4120*) tumor uptake was observed at all time-points. Image-derived biodistribution revealed a similar profile between randomly and site-specifically labeled [89]Zr-DFO-IgG1 with retention in blood, liver and kidneys slowly clearing throughout the imaging time-course (Figure S4C). *Ex vivo* biodistribution confirmed the *in vivo* imaging results and no difference in uptake was found between the probes (*p>0.6395*) except in the liver (*p=0.03*), Figure S4D.

Discussion

The remarkable ability of [89]Zr-labeled mAbs to monitor the performance of antibody-based therapeutics makes [89]Zr-immuno-PET a much-desired platform to predict the response to such agents, which are increasingly used in the clinic. This is true for both the drug development phase as well as an individual companion diagnostic. Accordingly, the significance of manufacturing more robust and reproducible conjugates by ways of specific labeling strategies becomes apparent. In the present study, the monoclonal antibody trastuzumab (Herceptin®) was used as a model antibody to assess the effect of site-specific radiolabeling on tumor uptake, biodistribution, stability and immuno-reactivity in a HER2-positive ovarian cancer mouse model.

Different strategies utilizing glycan remodeling by enzymatic approaches representing different degrees of modification were used to yield different conjugates. Initially, the conjugates were characterized *in vitro* and site-specific probes exhibited superior *in vitro* behavior with increased plasma stability and immuno-reactivity. The immuno-reactivity of the randomly labeled version was found to be 80%, which is in line with previous reports in the literature [5]. Preserved reactivity towards target is of outmost importance to reliably predict the distribution of the parent therapeutic antibody, emphasizing a clear benefit of site-specific labeling.

In the current study, site-specific versions by both the endoS2 and β-Gal method demonstrated significantly higher tumor uptakes when compared to the randomly labeled version. Tumor uptake in the SK-OV-3 model was nearly twice as high for the site-specific conjugates, 14.2 ± 1.7 %ID/g (β-Gal) and 16.7 ± 1.5 %ID/g (endoS2), compared to 6.5 ± 0.5 %ID/g for the random labeled trastuzumab 120 hours post-injection. In some preclinical model systems however, the site-specific approach for immuno-PET

imaging has not shown superiority to the traditional conjugation strategies [22,25,27]. One contributing factor could be the specific antibody and/or mouse model used. One could imagine, that the added value of a site-specifically mAb conjugated far from the antigen-binding region for *in vivo* PET imaging, is as diverse as the antibody itself. To our knowledge, this is the first report on the impact of site-specific labeling of trastuzumab by glycan remodeling for imaging purposes. Indeed, more antibodies need to be evaluated in order to support, confirm or refute that site-specific labeling in general will improve immuno-PET imaging.

In terms of accumulation in off-target organs, the four variants behaved similarly. Notably, the similar accumulation observed in bone between the probes highlights that the differences in stability cannot be credited to the transchelation of [89]Zr. A tendency towards higher retention of site-specific tracers in spleen and kidney was observed. Also, the *ex vivo* biodistribution data showed a significantly higher liver accumulation of site-specifically labeled (β-Gal) compared to randomly labeled [89]Zr-DFO-trastuzumab. Being major clearance routes for high-molecular weight complexes, the higher risk of aggregation when perturbing the glycosylation state [33] could be the reason for increased liver, kidney and spleen uptake for site-specific versions of [89]Zr-DFO-trastuzumab. Contrasting to this, is the increased blood pool of site-specific tracers compared to the randomly labeled version, and the higher activity is thus more likely to be attributed to the highly-perfused nature of these organs.

The PET imaging data was strongly supported by the *ex vivo* biodistribution data with major differences primarily in terms of tumor uptake. Moreover, the differences in blood pool at the 120-hour time-point is in line with the *in vitro* stability of compounds in plasma, indicative of site-specific tracers outperforming the randomly labeled version. With different labeling strategies and aiming for equal mass protein dose injected, we speculated whether the differential uptake pattern could be attributed to differences in specific activity. We therefore pursued the dose-escalation study. Co-injection with unlabeled trastuzumab did not considerably alter the distribution of [89]Zr-DFO-trastuzumab, randomly or site-specifically labeled. A tendency towards increased circulation time with increased dose was observed for all tracers, as expected for circulating IgGs. This was also confirmed by the tumor-to-blood ratios at different protein doses. Notably, the tumor uptake was unaffected of antibody dose, highlighting that the tumor uptake was not specific activity-dependent in the investigated range.

However, a blocking tendency was observed for endoS2 modified ^{89}Zr-DFO-trastuzumab with higher protein doses.

Compared to other immuno-PET radiotracers developed for targeting HER2, the observed tumor uptake for randomly labeled ^{89}Zr-DFO-trastuzumab (6.5 ± 0.5 %ID/g) is generally lower than previously reported. Dijkers et al. [5] stated a mean tumor uptake of 30-33 %ID/g in SK-OV-3 tumor-bearing xenografts 6 days post-injection. Likewise, Tinianow et al. [22] demonstrated a mean tumor uptake of 18.9-25.6 %ID/g in BT-474 (HER2 3+) xenografts 6 days post-injection. Despite these immediate differences in tumor uptake, the tumor-to-blood ratio of 6.5 observed 5 days post-injection (100 µg co-injection) in the present study is quite similar to the 7.6 and 5.1-7.1 observed 6 days post-injection as obtained by Dijkers and Tinianow, respectively. Furthermore, Dijkers et al. also found the tumor uptake to be independent of antibody dose in a similar range as we applied in this study.

With the noticeable impact of conjugation method on tumor uptake values, we were questioning whether this exclusively could be attributed to the differences in immuno-reactivity. The glycosylation state of the heavy chain N-linked glycans plays an important role in complement-dependent cytotoxicity (CDC) and antibody-dependent cell-mediated cytotoxicity (ADCC), through the Fcγ receptor (FcγR). Deglycosylated IgG no longer bind the FcγR and trigger CDC nor ADCC [34,35], opening an opportunity for site-specific trastuzumab by glycan modification alone to avoid immune recognition and reside in the blood for a prolonged period. The involvement of IgG-Fc in IgG recycling through the neonatal Fc receptor (FcRn) contrasts to this however, which is thought to be independent of Fc glycosylation [36]. To investigate the impact of enzymatic digest of the Fc glycans, we performed a control experiment with endoS2 representing the largest degree of modification in this study. The fact that endoS2 modification prior to random labeling did not result in superior tumor-targeting properties or distribution compared to the randomly labeled version, indicates that the major differences between the probes are to be found in the antigen-binding region. The flow cytometry of trastuzumab and DFO-trastuzumab (random, β-Gal and endoS2) slightly supported this notion with lowest K_D for randomly labeled trastuzumab, although the differences were not prominent.

Additional control experiments with an isotype control matched antibody supported the above-described findings of endoS2 modified and concurrently randomly labeled trastuzumab. Glycan modification of human IgG1 using endoS2 did not alter the distribution of tracer compared with randomly labeled IgG1 and the tumor uptake of both versions was low. This means that roughly ~3-4 %ID/g of the observed mean ^{89}Zr-DFO-trastuzumab uptake can be attributed to non-specific uptake or the enhanced permeability and retention (EPR) effect [37,38]. The *in vivo* biodistribution suggests that the ^{89}Zr-DFO-IgG1 tumor uptake is most likely due to the latter with uptake values similar to that of blood. These results are also in line with the tumor uptake of ^{89}Zr-DFO-trastuzumab (endoS2) in ST518 PDX tumors (~5 %ID/g) that are considered HER2 negative (HER2 0+).

The significance of site-specific labeling of mAbs extends beyond molecular imaging purposes. The synthesis and production of efficacious ADCs currently suffers from instability in the circulation and thus off-target toxicity as well as a large variation in cytotoxic payloads. In the case of trastuzumab-based ADCs, a trastuzumab-maytansine coupled by conventional lysine chemistry has been shown to exhibit a shorter biological half-life than various site-specific versions [39]. Indeed, the benefits of site-specific labeling are antibody-dependent. Nonetheless, by utilizing the site-specific approach the impact of introduction of a chelator on immuno-reactivity, stability and biodistribution is minimized. Adding to this, the site-specific methodology undeniably offers a route to reproducible, well-defined radioimmuno-conjugates for *in vivo* imaging.

Conclusions

To the best of our knowledge, this is the first report on the impact of site-specific labeling of trastuzumab by the SiteClick™ technology for immuno-PET. Site-specifically labeled ^{89}Zr-DFO-trastuzumab displayed good *in vitro* characteristics with increased stability and immuno-reactivity when compared to ^{89}Zr-DFO-trastuzumab conjugated by conventional lysine chemistry. Furthermore, site-specific ^{89}Zr-DFO-trastuzumab exhibited superior tumor-targeting properties in the SK-OV-3 model and was well-matched for the specific immuno-PET imaging of HER2-positive PDX tumors. ^{89}Zr-DFO-trastuzumab variants by the β-galactosidase and endoglycosidase S2 approach are suitable for clinical manufacturing and together, these findings support the further development of site-specifically radiolabeled mAbs for immuno-PET.

Abbreviations

%ID/g: injected dose per gram tissue; ^{89}Zr: zirconium-89; ADCC: antibody-dependent

cell-mediated cytotoxicity; ADCs: antibody-drug-conjugates; ANOVA: analysis of variance; BSA: bovine serum albumin; CDC: complement-dependent cytotoxicity; CT: computed tomography; DAB: 3,3′-Diaminobenzidin; DFO: desferrioxamine; DIBO-DFO: dibenzocyclooctyne-desferrioxamine; DMSO: dimethyl sulfoxide; endoS2-R: endoglycosidase S2-Random; EDTA: ethylenediaminetetraacetic acid; endoS2: endoglycosidase S2; EOS: end-of-synthesis; FACS: fluorescence activated cell sorting; FBS: fetal bovine serum; Fc: fragment crystallizable region; FcRn: fc recptor; FcγR: Fcγ receptor; GalT: galactose-1-phosphate uridyl transferase; HER2: human epidermal growth factor receptor 2; HPLC*:* high-performance liquid chromatography; IgG: immunoglobulin G; IHC: immunohistochemistry; IRF: immuno-reactive fraction; mAb: monoclonal antibody; MBq: mega becquerel; MFI: median fluorescent intensity; $MnCl_2$: manganese chloride; $NaHCO_3$: sodium bicarbonate; Na_2CO_3: sodium carbonate; NaCl: sodium chloride; PBS: phosphate buffered saline; PDX: patient-derived xenograft; PET: positron emission tomography; *p*-SCN-Bn-DFO: desferrioxamine-p-benzyl-isothio-cyanate; radio-TLC: radio-thin-layer chromatography; ROIs: region of interests; SEC-HPLC: size-exclusion chromatography – high-performance liquid chromatography; SEM: standard error of mean; ß-Gal: ß-(1-4) galactosidase; HRP: horseradish peroxidase; TBS: tris-buffered saline; TLC: thin-layer chromatography; UDP-GalNAz**:** uridine 5′-diphos-pho-N-azidoacetylgalactosamine tetraacylated.

Supplementary Material

Supplementary figures and table.
http://www.thno.org/v09p4409s1.pdf

Acknowledgements

The authors would like to thank Hanna Toftevall and colleagues at Genovis A/B for conducting the degree-of-labeling experiments. The authors would also like to acknowledge Camilla S. Knudsen and Michelle W. Kaijer for excellent technical assistance.

Competing Interests

The authors have declared that no competing interest exists.

References

1. Fleuren EDG, Versleijen-jonkers YMH, Heskamp S, Herpen CML Van, Oyen WJG, Graaf WTA Van Der, et al. Theranostic applications of antibodies in oncology. Mol Oncol. 2014;8:799-812.
2. Freise AC, Wu AM. In vivo imaging with antibodies and engineered fragments. Mol Immunol. 2015;67:142-152.
3. Perk LR, Vosjan MJWD, Visser GWM, Budde M, Jurek P, Kiefer GE, et al. p-Isothiocyanatobenzyl-desferrioxamine: a new bifunctional chelate for facile radiolabeling of monoclonal antibodies with zirconium-89 for immuno-PET imaging. Eur J Nucl Med Mol Imaging. 2010;37:250-259.
4. Sharma SK, Sevak KK, Monette S, Carlin SD, Knight JC, Wuest FR, et al. Preclinical 89Zr-immunoPET of high Grade serous ovarian cancer and lymph node metastasis. J Nucl Med. 2016;57:771-776.
5. Dijkers ECF, Kosterink JGW, Rademaker AP, Perk LR, van Dongen G a MS, Bart J, et al. Development and characterization of clinical-grade 89Zr-trastuzumab for HER2/neu immunoPET imaging. J Nucl Med. 2009;50:974-981.
6. Ulaner GA, Hyman DM, Lyashchenko SK, Lewis JS, Carrasquillo JA. 89Zr-Trastuzumab PET/CT for Detection of Human Epidermal Growth Factor Receptor 2–Positive Metastases in Patients With Human Epidermal Growth Factor Receptor 2–Negative Primary Breast Cancer. Clin Nucl Med. 2017;42:912-917.
7. Dijkers EC, Munnink THO, Kosterink JG, Brouwers AH, Jager PL, Jong JR De. Biodistribution of 89Zr-trastuzumab and PET Imaging of HER2-Positive Lesions in Patients With Metastatic Breast Cancer. Clin Pharmacol Ther. 2010;87:586-592.
8. Donoghue JAO, Lewis JS, Pandit-taskar N, Fleming SE, Der HS, Larson SM, et al. Pharmacokinetics, Biodistribution, and Radiation Dosimetry for 89Zr-Trastuzumab in Patients with Esophagogastric Cancer. J Nucl Med. 2018;59:161-167.
9. Deri MA, Zeglis BM. PET Imaging with 89Zr: From Radiochemistry to the Clinic. Nucl Med Biol. 2013;40:3-14.
10. Deri MA, Ponnala S, Zeglis BM, Pohl G, Dannenberg JJ, Lewis JS, et al. Alternative chelator for 89Zr radiopharmaceuticals: Radiolabeling and Evaluation of 3,4,3-(LI-1,2-HOPO). J Med Chem. 2014;57:4849-4860.
11. Guérard F, Lee Y-S, Brechbiel MW. Rational design, synthesis and evaluation of tetrahydroxamic acid chelators for stable complexation of ZrIV. Chemistry (Easton). 2014;20:5584-5591.
12. Adumeau P, Sharma SK, Brent C, Zeglis BM. Site-Specifically Labeled Immunoconjugates for Molecular Imaging-Part 1: Cysteine Residues and Glycans. Mol Imaging Biol. 2016;18:1-17.
13. Agarwal P, Bertozzi CR. Site-Specific Antibody-Drug conjugates: The Nexus of Bioorthogonal Chemistry, Protein Engineering, and Drug Development. Bioconjug Chem. 2015;26:176-192.
14. Beck A, Goetsch L, Dumontet C, Corvaïa N. Strategies and challenges for the next generation of antibody–drug conjugates. Nat Rev Drug Discov. 2017;16:315-337.
15. Behrens CR, Liu B. Methods for site-specific drug conjugation to antibodies. MAbs. 2017;6:46-53.
16. Junutula JR, Raab H, Clark S, Bhakta S, Leipold DD, Weir S, et al. Site-specific conjugation of a cytotoxic drug to an antibody improves the therapeutic index. Nat Biotechnol. 2008;26:925-932.
17. Geel R Van, Wijdeven MA, Heesbeen R, Verkade JMM, Wasiel AA, Berkel SS Van, et al. Chemoenzymatic Conjugation of Toxic Payloads to the Globally Conserved N-Glycan of Native mAbs Provides Homogeneous and Highly Efficacious Antibody−Drug Conjugates. Bioconjug Chem. 2015;26:2233-2242.
18. Tait JF, Smith C, Levashova Z, Patel B, Blankenberg FG. Improved Detection of Cell Death In Vivo with Annexin V Radiolabeled by Site-Specific Methods. J Nucl Med. 2006;47:1546-1554.
19. Tavaré R, Wu WH, Zettlitz KA, Salazar FB, McCabe KE, Marks JD, et al. Enhanced immunoPET of ALCAM-positive colorectal carcinoma using site-specific 64Cu-DOTA conjugation. Protein Eng Des Sel. 2014;27:317-324.
20. Kijanka M, Warnders F, Khattabi M El. Rapid optical imaging of human breast tumour xenografts using anti-HER2 VHHs site-directly conjugated to IRDye 800CW for image-guided surgery. Eur J Nucl Med Mol Imaging. 2013;40:1718-1729.
21. Meimetis LG, Boros E, Carlson JC, Ran C, Caravan P, Weissleder R. Bioorthogonal Fluorophore Linked DFO-Technology Enabling Facile Chelator Quantification and Multimodal Imaging of Antibodies. Bioconjug Chem. 2016;27:257-263.
22. Tinianow JN, Gill HS, Ogasawara A, Flores JE, Vanderbilt AN, Luis E, et al. Site-specifically 89Zr-labeled monoclonal antibodies for ImmunoPET. Nucl Med Biol. 2010;37:289-297.
23. Zeglis BM, Mohindra P, Weissmann GI, Divilov V, Hilderbrand SA, Weissleder R, et al. Modular Strategy for the Construction of Radiometalated Antibodies for Positron Emission Tomography Based on Inverse Electron Demand Diels-Alder Click Chemistry. Bioconjug Chem. 2011;22:2048-2059.

24. Alt K, Paterson BM, Westein E, Rudd SE, Poniger SS, Jagdale S, et al. A Versatile Approach for the Site-Specific Modification of Recombinant Antibodies Using a Combination of Enzyme-Mediated Bioconjugation and Click Chemistry **. Angew Chem Int Ed Engl. 2015;54:7515-7519.

25. Zeglis BM, Davis CB, Aggeler R, Kang HC, Chen A, Agnew BJ, et al. Enzyme-Mediated Methodology for the Site-Specific Radiolabeling of Antibodies Based on Catalyst-Free Click Chemistry. Bioconjug Chem. 2013;24:1057-1067.

26. Zeglis BM, Davis CB, Abdel-Atti D, Carlin SD, Chen A, Aggeler R, et al. Chemoenzymatic Strategy for the Synthesis of Site-Specifically Labeled Immunoconjugates for Multimodal PET and Optical Imaging. Bioconjug Chem. 2014;25:2123-2128.

27. Houghton JL, Zeglis BM, Abdel-Atti D, Aggeler R, Sawada R, Agnew BJ, et al. Site-specifically labeled CA19.9-targeted immunoconjugates for the PET, NIRF, and multimodal PET/NIRF imaging of pancreatic cancer. Proc Natl Acad Sci U S A. 2015;112:15850-15855.

28. Schjoeth-Eskesen C, Nielsen CH, Heissel S, Højrup P, Hansen R, Gillings N, et al. [64 Cu]-labelled trastuzumab: optimisation of labelling by DOTA and NODAGA conjugation and initial evaluation in mice. J Labelled Comp Radiopharm. 2015;58:227-233.

29. Lindmo T, Boven E, Cuttitta F, Fedorko J, Bunn P. Determination of the Immunoreactive Fraction of Radiolabeled Monoclonal Antibodies by Linear Extrapolation to Binding at Infinite Antigen Excess. J Immunol Methods. 1984;72:77-89.

30. Dako. HercepTestTM Interpretation Manual - Breast Cancer. 2014:16-18.

31. Chang AJ, DeSilva R, Jain S, Lears K, Rogers B, Lapi S. 89Zr-Radiolabeled Trastuzumab Imaging in Orthotopic and Metastatic Breast Tumors. Pharmaceuticals (Basel). 2012;5:79-93.

32. Gaykema SBM, Schröder CP, Vitfell-Rasmussen J, Chua S, Munnink THO, Brouwers AH, et al. 89Zr-trastuzumab and 89Zr-bevacizumab PET to Evaluate the Effect of the HSP90 Inhibitor NVP-AUY922 in Metastatic Breast Cancer Patients. Clin Cancer Res. 2014;20:3945-3955.

33. Zheng K, Bantog C, Bayer R. The impact of glycosylation on monoclonal antibody conformation and stability. MAbs. 2011;3:568-576.

34. Nose M, Wigzell H. Biological significance of carbohydrate chains on monoclonal antibodies. Proc Natl Acad Sci U S A. 1983;80:6632-6636.

35. Jefferis R. Recombinant antibody therapeutics : the impact of glycosylation on mechanisms of action. Trends Pharmacol Sci. 2009;30:356-362.

36. Reusch D, Tejada ML. Fc glycans of therapeutic antibodies as critical quality attributes. Glycobiology. 2015;25:1325-1334.

37. Maeda H, Matsumura Y. A New Concept for Macromolecular Therapeutics in Cancer Chemotherapy: Mechanism of Tumoritropic Accumulation of Proteins and the Antitumor Agent Smancs. Cancer Res. 1986;46:6387-6392.

38. Fang J, Nakamura H, Maeda H. The EPR effect: Unique features of tumor blood vessels for drug delivery, factors involved, and limitations and augmentation of the effect. Adv Drug Deliv Rev. 2011;63:136-151.

39. Drake PM, Albers AE, Baker J, Banas S, Bar RM, Bhat AS, et al. Aldehyde Tag Coupled with HIPS Chemistry Enables the Production of ADCs Conjugated Site-Specifically to Different Antibody Regions with Distinct in Vivo Efficacy and PK Outcomes. Bioconjug Chem. 2014;25:1331-1341.